X-ray spectromicroscopic investigation of natural organochlorine distribution in weathering plant material

Alessandra C. Leri [a,*], Matthew A. Marcus [b], Satish C.B. Myneni [c,d]

[a] *Department of Chemistry, Princeton University, Princeton, NJ 08544, USA*
[b] *Advanced Light Source, Lawrence Berkeley National Laboratory, Berkeley, CA 94720, USA*
[c] *Department of Geosciences, Princeton University, Guyot Hall, Princeton, NJ 08544, USA*
[d] *Earth Sciences Division, Lawrence Berkeley National Laboratory, Berkeley, CA 94720, USA*

Abstract

Natural organochlorine (Cl_{org}) is ubiquitous in soil humus, but the distribution and cycling of different Cl species during the humification of plant material is poorly understood. Our X-ray spectromicroscopic studies indicate that the distributions of Cl_{org} and inorganic Cl^-(Cl_{inorg}) in oak leaf material vary dramatically with decay stage, with the most striking changes occurring at the onset of weathering. In healthy or senescent leaves harvested from trees, Cl_{inorg} occurs in sparsely distributed, highly localized "hotspots" associated with trichomes as well as in diffuse concentration throughout the leaf tissue. The Cl_{inorg} associated with trichomes exists either in H-bonded form or in a solid salt matrix, while the Cl_{inorg} in diffuse areas of lower Cl concentration appears exclusively in H-bonded form. Most solid phase Cl_{inorg} leaches from the leaf tissue during early weathering stages, whereas the H-bonded Cl_{inorg} appears to leach away slowly as degradation progresses, persisting through advanced weathering stages. In unweathered leaves, aromatic and aliphatic Cl_{org} were found in rare but concentrated hotspots. In weathered leaves, by contrast, aromatic Cl_{org} hotspots are prevalent, often coinciding with areas of elevated Fe or Mn concentration. Aromatic Cl_{org} is highly soluble in leaves at early weathering stages and insoluble at more advanced stages. These results, combined with optical microscopy, suggest that fungi play a role in the production of aromatic Cl_{org} in weathering leaf material. Aliphatic Cl_{org} occurs in concentrated hotspots in weathered leaves as well as in diffuse areas of low Cl concentration. The distribution and speciation of Cl in weathering oak leaves depicted by this spectromicroscopic study provides new insight into the formation and cycling of Cl_{org} during the decay of natural organic matter.

1. INTRODUCTION

Until the late 1980s, Cl was believed to exist primarily in the form of stable inorganic chloride (Cl_{inorg}) in uncontaminated terrestrial systems. The investigation of organochlorine (Cl_{org}) molecules in environmental systems mainly focused on persistent, toxic anthropogenic pollutants such as pesticides and disinfection byproducts. Cl_{inorg} was (and often still is) presumed sufficiently unreactive in soil environments for use as a tracer in hydrological studies (Christophersen and Neal, 1990; Derby and Knighton, 2001). Recent studies using the adsorbable organohalogen (AOX) sum parameter technique (Asplund et al., 1989; Asplund and Grimvall, 1991) and X-ray spectroscopy (Myneni, 2002a; Leri et al., 2006) revealed Cl_{org} to be surprisingly prevalent in forest soils, appearing in concentrations too high to be ascribed to anthropogenic sources.

Hardly inert, Cl_{inorg} undergoes transformations to Cl_{org} as part of a complex, poorly understood biogeochemical cycle in soil systems (Öberg, 1998, 2002). Cl_{inorg} enters the soil primarily through atmospheric deposition and litterfall. Aqueous soil Cl_{inorg} is subject to uptake by plants via the

* Corresponding author. Present address: Marymount Manhattan College, Department of Natural Sciences and Mathematics, 221 E 71st Street, New York, NY 10021, USA. Fax: +1 212 517 0528.

E-mail address: aleri@mmm.edu (A.C. Leri).

root system and translocation within the plant tissues (White and Broadley, 2001). In addition to contributing Cl_{inorg} to the soil, litterfall may represent a substantial source of Cl_{org} to soil systems (Öberg and Grøn, 1998; Öberg et al., 2005); various individual Cl_{org} compounds have been isolated from the tissues of higher plants (Engvild, 1986). Small amounts of Cl_{org} likely enter the soil through atmospheric deposition as well (Asplund et al., 1989). However, Cl_{org} concentrations measured in the soil are believed to exceed contributions from litterfall and atmospheric deposition. Studies have shown that soil Cl_{org} is correlated with total organic carbon (Johansson et al., 2003). This correlation and numerous studies linking Cl_{org} with decaying organic material have led to the reigning hypothesis that much of the natural Cl_{org} in soil is produced from Cl_{inorg} during the degradation of plant matter (Hjelm et al., 1995; Flodin et al., 1996; Öberg et al., 1996; Myneni, 2002a; Öberg, 2002).

The mechanistic origin(s) of natural Cl_{org} remains unclear because the degradation of plant matter in soil is a complicated process, mediated by diverse microorganisms and subject to the effects of photodegradation and leaching. The leaching and biochemical alteration of plant material during natural degradative processes will be hereafter referred to as "weathering". Haloperoxidative conditions have been shown to exist in soil systems, possibly due to the activity of enzymes that produce extracellular reactive halogen species, such as hypochlorous acid, from inorganic halides (Asplund et al., 1993; Laturnus et al., 1995). Commercial chloroperoxidase (CPO), a haloperoxidase enzyme isolated from source fungi, has proved capable of chlorinating non-specific phyto-organic molecules (Reina et al., 2004) and fulvic acid moieties (Niedan et al., 2000). Ligninolytic ascomycetes fungi display CPO activity and chlorinate aromatic lignin structures as they break down plant material (Ortiz-Bermúdez et al., 2007). Such fungi are omnipresent in soil systems and probably make significant contributions to the global Cl_{org} pool. In addition to these non-specific natural chlorination products, individual chlorinated metabolites have been isolated from soil fungi and lichen for decades (Yosioka et al., 1968; Turner and Aldridge, 1983; Wijnberg, 1998; Gribble, 2003). Abiotic (non-enzymatic) chlorination has also been shown to occur naturally and is thought to be catalyzed by metal ions in the low-pH soil environment (Keppler et al., 2000; Schoeler and Keppler, 2002; Fahimi et al., 2003; Holmstrand et al., 2006).

This evidence collectively indicates that terrestrial Cl undergoes complex biogeochemical transformations. The processes leading to the formation of Cl_{org} in weathering plant material are poorly understood, due primarily to the heterogeneity of natural organic matter (NOM), which is a complex chemical mixture of the low and high molecular weight organic molecules that compose weathering plant material. NOM encompasses a variety of functional groups, including carboxyls, phenolics, hydroxyls, amides, and amines, exhibiting little typical or predictable structure. This complexity makes it difficult to detect chlorinated moieties, much less unravel the key mechanisms in the natural production of Cl_{org}.

Using sensitive spectroscopic tools, we conducted an *in situ* investigation of Cl distribution and speciation in oak leaves at different weathering stages. The current study builds from Myneni's use of X-ray absorption near-edge structure (XANES) spectroscopy to determine the bulk speciation of Cl in chemically heterogeneous environmental samples (Myneni, 2002a). Unlike the AOX technique, synchrotron-based XANES spectroscopy requires only minimal physical sample preparation, shrinking the risk of inadvertent "benchtop" chlorination. XANES spectroscopy is element-specific and sensitive to all forms of Cl, allowing Cl to be probed directly in complex chemical mixtures such as NOM (Myneni, 2002b). This method ensures a complete portrait of Cl speciation, detecting forms of Cl that the AOX method may overlook, such as unextractable chlorinated macromolecules.

We have applied Cl 1*s* XANES spectroscopy to the investigation of Cl speciation in weathering plant material on both macro- and micro-scopic scales. Previous bulk (macro) Cl 1*s* XANES spectroscopic studies revealed that the Cl in healthy or senescent oak leaves collected from trees exists primarily in the form of Cl_{inorg}. By contrast, weathered oak leaves from the mulch on the forest floor tend to display strong aromatic and aliphatic Cl_{org} components in addition to Cl_{inorg} (Myneni, 2002a). In this report, we document the micro-scale heterogeneities in Cl distribution and speciation observed using X-ray spectromicroscopic techniques. X-ray spectromicroscopy merges XANES spectroscopy with micro-X-ray fluorescence (μ-XRF) mapping of different elements in a sample using a micro-focused beam with a spot size as small as several μm^2. This technique illuminates chemical microenvironments, providing a more detailed picture than macro-scale analysis by revealing the spatial distribution of various Cl species. Also, through the simultaneous mapping of numerous elemental distributions, μ-XRF uncovers interrelationships among elements. Correlations between Cl_{org} and other elements, particularly metals, are potentially relevant to the identification of biotic and abiotic chlorination mechanisms.

The spectromicroscopic results presented here reveal distinct fractions of Cl_{org} and Cl_{inorg} associated with different weathering stages in plant material. Although not quantitative, this dataset clearly demonstrates the diminution of Cl_{inorg} species and the emergence of concentrated regions of Cl_{org} in leaf material as a result of decay processes. In many cases, we have been able to link Cl_{org} with other elements such as Fe or Mn, or with microbiological activity on the leaf surface, providing clues as to the genesis of Cl_{org}. These spectromicroscopic data shed new light on the processes underlying Cl_{org} production in the humifying plant material of the soil organic horizon.

2. MATERIALS AND METHODS

2.1. Sampling site

Oak leaf samples of various tree species, mainly white oak (*Quercus alba*), chestnut oak (*Quercus prinus*), black oak (*Quercus velutina*), and Southern red oak (*Quercus fal-*

cata), were collected from the Brendan Byrne State Forest in the Pine Barrens of New Jersey, USA (39°53′N, 74°30′W). This area had a mean annual temperature of 12.2°C and 120 cm of annual precipitation in 2002, according to the National Climate Data Center. The proximity of this sampling site to the ocean (~30 km) guarantees significant Cl_{inorg} inputs to soil and plants from atmospheric deposition. Mean annual Cl_{inorg} deposition in this forest was 0.515 mg/L in 2002, according to the New Jersey Department of Environmental Protection. The soil in this forest is sandy and acidic (pH 3.5–5.5) and tends to be well-drained (Boyd, 1991), so that there is little accumulation of nutrients and NOM in the A-horizon.

The vegetation in the Brendan Byrne State Forest is dominated by oak and pine trees of various species. Unweathered oak leaves were harvested from trees in the mid-fall prior to abscission. Oak leaf mulch material was also collected from the forest floor at different points throughout the year to represent progressive weathering stages. The leaf litter on the floor of this forest occurs in two to three distinct layers depending on the season. Each mulch layer roughly corresponds to one season's litter deposition. Thus, the topmost layer represents material from the most recent litterfall (which is thus the least weathered), the middle layer the previous year's deposition, and the bottommost layer that of two years prior (the most degraded leaf litter). After more than three years of weathering on the forest floor, the litter exists in a highly humified state, decomposed to the extent that individual leaf species are no longer discernible. Weathering times for leaf litter samples collected from the forest floor are estimated based on mulch layer position and an assumed abscission date of October 1.

2.2. Experimental field station

Controlled experiments on oak leaf degradation were conducted on detached senescent leaves in trays located in the Brendan Byrne State Forest in relatively open areas apart from the tree canopy. Multiple species of senescent oak leaves were harvested on October 31, 2003, from trees in the vicinity of the field experimental apparatus, with the objective to collect substrates representative of the season's litterfall prior to contact with the ground. Leaves were placed in field station trays to begin the weathering experiment on November 16, 2003. The trays were suspended approximately 1.5 m above the soil surface with the intention of limiting the access of the soil microbial community to the weathering leaves, thus enabling a semi-abiotic study of leaf degradation. Leachate resulting from the interaction of rainwater with the weathering leaves was routed from the trays into carboys.

Experimental trays consisted of polypropylene plastic and contained a layer of coarse polypropylene mesh on which the weathering oak leaves rested. A fine polypropylene mesh fitted over the tops of the trays prevented the loss of experimental substrates and the entry of extraneous solid material. This mesh was secured over the trays with nylon string and was easily removable for sampling purposes. Plant material from the experimental trays was periodically sampled for spectroscopic analysis.

2.3. X-ray microanalysis and Cl 1s XANES spectroscopy

μ-XRF experiments were performed on beamline 10.3.2 (Marcus et al., 2004) at the Advanced Light Source (ALS) at Lawrence Berkeley National Laboratory (LBNL, Berkeley, CA, USA). Detection of elements with atomic numbers lower than 18 was enabled using a He-purged air exclusion device fitted with X-ray clean polyfilm windows over the 7-element solid-state Ge detector. Natural samples were analyzed *in situ* with no chemical preparation aside from aqueous rinsing in select cases. Samples were mounted using Kapton tape on metal alloy sample holders designed to fit the movable stage in the beam path. Once samples were mounted on the stage, optimal focus was achieved before moving in the detector so that approximately 1 mm of space remained between the air exclusion device and the sample stage, allowing the stage to move freely while minimizing the air in the beam path. Samples were exposed directly to the incoming X-ray beam at a 45° angle. The detector was oriented at 90° from the X-ray beam in the plane of the sample. Once the detector was moved into position, an Al sheath was fitted over the sample mount and a Cl 1*s* XANES spectrum collected to evaluate the possibility of Cl contamination in the beam path (the epoxy used to assemble the air exclusion device, for instance, contains high levels of Cl_{org}). If necessary, the detector position was adjusted until the beam path proved free of Cl contamination. The Al sheath was removed prior to mapping the sample.

Elemental maps of oak leaf surfaces were collected exciting at 50 eV below the Ar K-edge to minimize the fluorescence signal of atmospheric Ar, which overlaps with that of Cl. For μ-XRF mapping, the monochromator was detuned until the I_0 signal intensity was reduced by 50% then retuned slightly to leak in minimal higher order harmonics. This leakage allowed elements above Ar such as Ca, Fe, and Mn to appear in the maps with some attenuated intensity. The X-ray beam size was set to 16 (horizontal) × 7 (vertical) μm^2. μ-XRF maps were acquired with step sizes varying from 15 to 20 μm, depending on the desired degree of sampling, and processed using the XY-mapping software associated with beamline 10.3.2.

For Cl 1*s* μ-XANES spectral acquisition, the monochromator was detuned to halve the maximum I_0 intensity at 2860 eV, fully screening out high-order harmonics to maximize spectral quality. Sample fluorescence was measured over an energy range of 2800–2860 eV. Cl 1*s* μ-XANES spectra were acquired using a 0.08 eV step size around the edge and 0.1–0.5 eV step sizes above and below the edge. The energy of the monochromator was calibrated to the discrete absorption maximum in the Cl 1*s* XANES spectrum of chlorophenol red defined at 2821.2 eV.

Cl 1*s* XANES data were processed using EXAFS Editor, WinXAS version 2.0 (Ressler, 1998), and PeakFit version 4.0 (Bergbreiter and Srinivas, 1992). EXAFS Editor, a data analysis utility associated with beamline 10.3.2, was used for preliminary inspection, deadtime correction, and averaging of fluorescence scans. Averaged scans were imported into WinXAS for energy calibration, background subtraction, and normalization. A smooth background

was obtained by fitting a first-order polynomial to the pre-edge region, and the edge jump was normalized to 1.0 with another first-order polynomial fit to the post-edge region. This normalization allows for comparative analysis of spectral features in the near-edge region, where absorption intensity is dependent on Cl speciation. WinXAS was also used for linear least squares fitting of sample spectra with data from model chemical compounds to establish the speciation of Cl. PeakFit was used for deconvolution of spectra into their component peaks.

Cl 1*s* XANES spectral features vary according to the coordination environment of Cl (Fig. 1). Inorganic and organic forms of Cl can be readily distinguished. Compared with Cl_{inorg} compounds (Fig. 1D–G), Cl_{org} compounds have intense low-energy peaks corresponding to electronic transitions from the 1*s* orbital to π^* and σ^* molecular orbitals (Fig. 1A–C). The C–Cl bond length determines the energy of this low-energy absorption maximum: Cl atoms bound to aromatic carbon, as in tetrachlorophenol and chlorophenol red (Fig. 1A and B), have absorption maxima occurring ~0.6 eV higher than those of aliphatic Cl_{org} such as chlorodecane (Fig. 1C).

Certain post-edge characteristics in the aromatic Cl_{org} spectra appear to be related to the degree of chlorination of the aromatic ring. Tetrachlorophenol (Fig. 1A), with four Cl atoms on the ring, and chlorophenol red (Fig. 1B), with one Cl per ring, display absorption maxima at similar energies, 2821.1 and 2821.2 eV, respectively. Full spectral deconvolution reveals two contributing Gaussians at ~2825.2 and ~2827.8 eV in the post-edge region of both the tetrachlorophenol and chlorophenol red spectra (Reina et al., 2004). However, the Gaussian at 2825.2 eV in the tetrachlorophenol spectrum is sharper and higher in amplitude than the analogous feature in the chlorophenol red spectrum, resulting in more pronounced structure in the post-edge region of the tetrachlorophenol spectrum compared with the broader features in the post-edge region of the chlorophenol red spectrum.

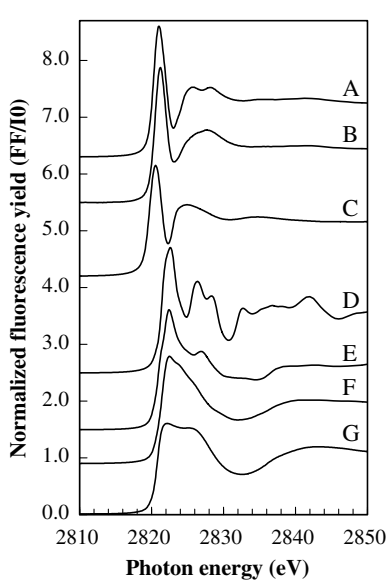

Fig. 1. Normalized Cl 1s XANES spectra of organic and inorganic Cl model compounds. (A) tetrachlorophenol (aromatic Cl_{org}, multiply chlorinated ring); (B) chlorophenol red (aromatic Cl_{org}, singly chlorinated ring); (C) chlorodecane (aliphatic Cl_{org}); (D) solid KCl (solid phase Cl_{inorg}); (E) solid trizma–HCl (H-bonded Cl_{inorg}); (F) solid glycine–HCl (H-bonded Cl_{inorg}); (G) aqueous HCl (hydrated Cl_{inorg}).

In addition to differentiation of Cl_{org} forms, Cl 1*s* XANES spectra allow different types of Cl_{inorg} to be recognized based on their post-edge features. Spectra of Cl_{inorg} in solid matrices tend to display distinct structural features because the compounds are highly ordered, as in the KCl (s) spectrum (Fig. 1D). Hydrogen-bonded Cl_{inorg} in the solid phase, as in trizma–HCl (s) and glycine–HCl (s), yields Cl 1*s* XANES spectra that are a combination of sharp features that can be pronounced enough to appear as post-edge shoulders (Fig. 1E and F). By contrast, H-bonded Cl_{inorg} in the aqueous phase, as in HCl (aq), gives spectra with broader features (Fig. 1G).

In environmental sample spectra, the relative proportions of Cl_{inorg}, aliphatic Cl_{org}, and aromatic Cl_{org} were determined by least-squares fitting sample spectra with spectra of representative model compounds such as those in Fig. 1 (Myneni, 2002a; Leri et al., 2006). The errors in fitting fell under 10%.

2.4. Fungal inoculation studies

The fungus *Fusarium oxysporum sp*. (Carolina Biological Supply) was cultivated in potato dextrose broth at 25 °C, yielding a suspension. Healthy white oak leaves freshly harvested from trees in the Brendan Byrne State Forest were washed with deionized H_2O, sectioned, and inoculated with the fungal suspension in moist Petri dishes, following an established procedure (Monde et al., 1998). The inoculated leaves were incubated for two weeks at 25 °C prior to X-ray analysis.

2.5. Scanning electron microscopy (SEM)

Following μ-XRF analysis, the oak leaf surfaces were examined using a high-resolution FEI XL30 FEG-SEM system with a 10 kV accelerating voltage. Samples were coated with Au prior to SEM analysis using a VCR IBS/TM250 Ion Beam Sputterer.

3. RESULTS AND DISCUSSION

3.1. Distribution and speciation of Cl in oak leaves

Imaging with μ-XRF reveals distinct microenvironments in weathering oak leaves. The emission energies of Cl and its periodic neighbor, S, are too close to resolve with the Ge detector. The signal from the S Kβ line at 2464 eV leaks into the Cl channel, so S-rich areas of a sample appear to contain Cl as well, which is problematic since NOM samples typically contain high S concentrations. To distinguish Cl from S in μ-XRF images, S intensity is shown in green along with Cl (red). Thus, Cl appears yellow–red (red + green), while S alone appears green. μ-XRF studies indicate

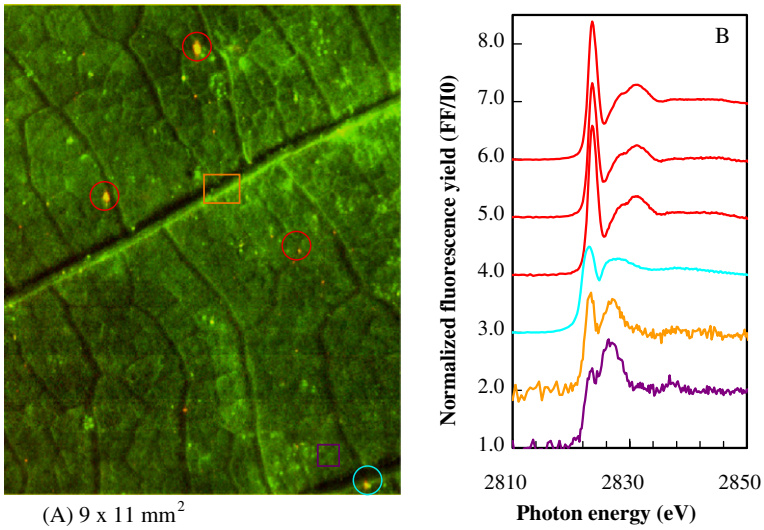

Fig. 2. (A) μ-XRF map of a weathered chestnut oak leaf from the forest floor mulch (estimated weathering time of approximately 5 months). Green = S Kα; red = Cl Kα. Lighter color corresponds to greater fluorescence intensity, i.e., greater elemental concentration. (B) Normalized Cl 1*s* XANES spectra corresponding to the circled/boxed areas in (A). Colors of circles/boxes in A match colors of associated spectra. Red spectra = aromatic Cl_{org}; turquoise spectrum = aliphatic Cl_{org}; orange/violet spectra = mixed aliphatic Cl_{org}/Cl_{inorg}.

that Cl is heterogeneously distributed in leaf tissue. For example, in the μ-XRF map of a weathered chestnut oak leaf from the topmost layer of mulch (estimated weathering time of approximately five months), Cl appears at highest concentration in localized hotspots as large as several hundred μm^2 in area (Fig. 2A). These Cl hotspots are scattered among diffuse areas of relatively low Cl concentration in the bulk of the leaf tissue. Cl hotspots similar to these in size and fluorescence intensity are observed in oak leaves at all weathering stages, although they are far less common in unweathered leaves harvested from trees. In unweathered leaves, Cl tends to appear in a more uniform distribution, spread throughout diffuse areas of low to moderate Cl intensity rather than concentrated in hotspots.

The combination of μ-XRF mapping and Cl 1*s* μ-XANES spectroscopy reveals the spatial distribution of different chemical forms of Cl (Fig. 2). Most Cl hotspots in the weathered chestnut oak leaf produced identical aromatic Cl_{org} μ-XANES spectra (Fig. 2B). The well-defined structural features in the post-edge region of these spectra suggest a polychlorinated aromatic structure. A limitation of XANES spectroscopy is that it only reveals the immediate coordination environment of the element of interest, meaning that we are unable to discern whether the observed polychlorinated aromatics are relatively low molecular weight molecules or part of a more substantial macromolecular structure, such as lignin or humic acid.

A small fraction of the Cl hotspots probed in this sample displayed strongly aliphatic Cl_{org} features (Fig. 2B). The aliphatic Cl_{org} spectra showed X-ray beam-induced dechlorination scan-to-scan, suggesting an unstable Cl_{org} compound. The diffuse areas of relatively low Cl concentration were also analyzed for Cl speciation. On the leaf vein, Cl speciation is predominantly aliphatic Cl_{org} (~60%), with Cl_{inorg} constituting the remainder (Fig. 2B). In areas of low Cl concentration apart from the veins, the Cl speciation breakdown is consistently ~40% aliphatic Cl_{org} and ~60% Cl_{inorg} (Fig. 2B). The aliphatic Cl_{org} in areas of relatively low Cl concentration appears stable in the X-ray beam, in contrast with the concentrated aliphatic Cl_{org} hotspots.

The emergent themes from the spectromicroscopic analysis of this weathered chestnut oak leaf are that the distribution of Cl species is heterogeneous and includes: (1) sparsely distributed but extremely intense aromatic Cl_{org} hotspots; (2) less frequent but similarly intense aliphatic Cl_{org} hotspots; and (3) low but fairly uniform background concentrations of aliphatic Cl_{org} and Cl_{inorg} on the leaf veins and throughout the leaf tissue. Such Cl μ-speciation results are emblematic of oak leaves at intermediate weathering stages and are consistent among all oak species examined. Noteworthy variations in Cl μ-speciation were found to occur as a function of oak leaf weathering stage.

Fig. 3. μ-XRF maps (left) and normalized Cl 1*s* XANES spectra (right) of white oak leaves at progressive weathering stages. In μ-XRF maps, lighter color indicates greater fluorescence intensity, i.e., greater elemental concentration. Green = S Kα; blue = Ca Kα red = Cl Kα. Colors of hollow shapes on μ-XRF maps match colors of associated XANES spectra. (A and B) Unweathered white oak leaf collected from tree at onset of senescence. Protuberances on surface correspond to trichomes. (C and D) Lightly weathered white oak leaf (weathering time: 2.5 weeks in field station apparatus removed from soil mulch). (E and F) Highly weathered white oak leaf (estimated weathering time of approximately 2 years on forest floor). The light-colored swath across the central area of the map represents an area that has been more extensively leached than the surrounding tissue. Cl speciation is color-coded: turquoise spectra = aliphatic Cl_{org}; red spectra = aromatic Cl_{org}; pink spectra = solid Cl_{inorg}; green spectra = H-bonded Cl_{inorg}; orange spectrum = mixed aliphatic Cl_{org} and Cl_{inorg}.

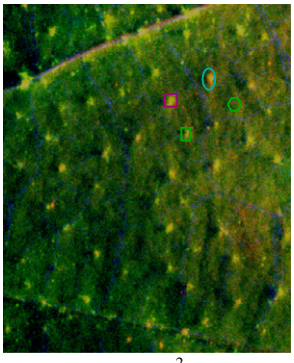

(A) 5 x 6 mm^2

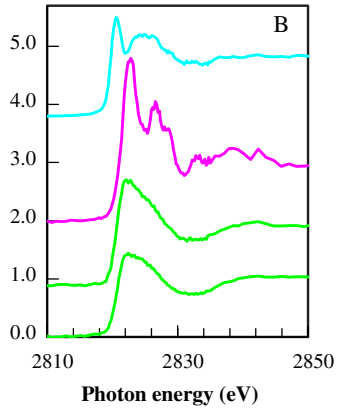

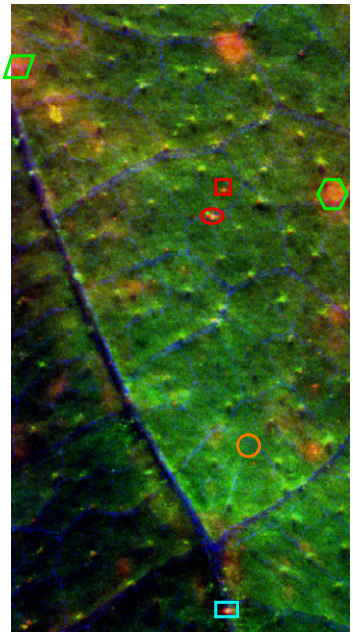

(C) 6 x 11 mm^2

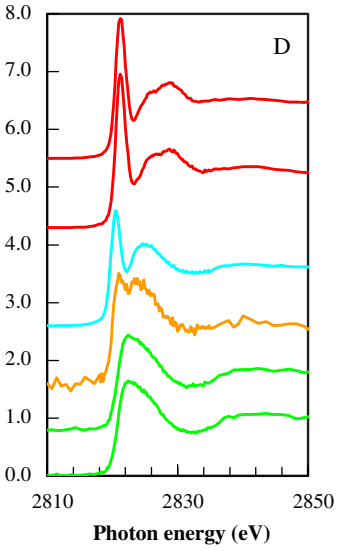

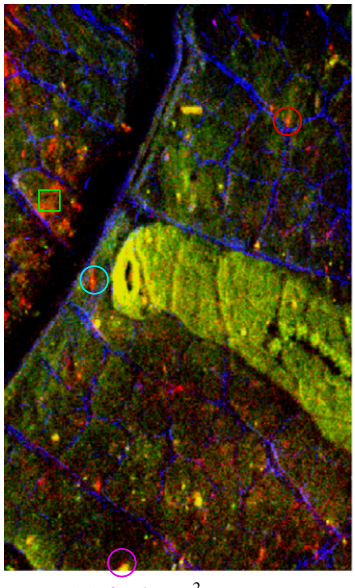

(E) 6 x 8 mm^2

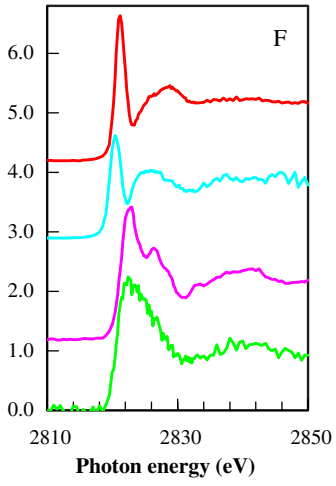

3.2. Variations in Cl distribution and speciation as a function of weathering time

Oak leaves at progressive weathering stages were subjected to X-ray spectromicroscopic analysis (Fig. 3). The distribution of assorted Cl species was found to vary dramatically according to degree of weathering, with the most dramatic differences emerging in the earliest weathering stages.

μ-XRF images of fresh leaves harvested from the trees at the onset of senescence typically display a fairly uniform distribution of similarly sized Cl hotspots (Fig. 3A). Optical microscopic observations (see Section 3.6 and Fig. 8A and B) indicate that these spots are associated with protuberant trichomes—epidermal leaf hairs associated with defensive as well as glandular functions. In these leaves, most Cl hotspots and diffuse areas of low Cl concentration produce Cl 1*s* μ-XANES spectra corresponding to H-bonded Cl_{inorg} (Fig. 3B). In addition, certain Cl hotspots yield Cl_{inorg} spectra with pronounced features characteristic of Cl_{inorg} in a highly ordered solid matrix (Fig. 3B). These spectra bear a close resemblance to that of KCl (s) (Fig. 1D), which provides a considerably more accurate match than other Cl_{inorg} salts in our spectral library, such as NaCl (s), $FeCl_3$ (s), and $AlCl_3$ (s), or transition metal tetrachloride salts that have been analyzed by other researchers (Shadle et al., 1995). It seems possible that these distinctive solid phase Cl_{inorg} spectra derive from salts that have crystallized on the leaf surface following glandular excretion. Epidermal salt glands are known to be associated with trichomes in numerous plant species (Thomson and Healey, 1984). It is also conceivable that this solid phase Cl_{inorg} represents some component of the epicuticular wax crystals that protect the leaf surface, the structure of which is poorly understood. Such distinctive μ-XANES spectra are less commonly observed in weathered leaves, even in the first months of weathering, suggesting that this solid form of Cl_{inorg} is easily degradable or leachable. Unweathered oak leaves also display occasional aliphatic Cl_{org} hotspots (Fig. 3B) that are prone to rapid X-ray beam damage. Aromatic Cl_{org} hotspots were rarely observed in unweathered leaves.

Tree-harvested unweathered oak leaves, such as the one described in Fig. 3A and B, represent the starting substrates for our controlled field weathering experiments. After 2.5 weeks of weathering in the above-ground field experimental apparatus, significant changes in Cl μ-speciation are apparent (Fig. 3C and D). There is a profusion of aromatic and aliphatic Cl_{org} hotspots in these samples (Fig. 3D). As with the unweathered sample, the aliphatic Cl_{org} spectra show X-ray beam-induced dechlorination scan-to-scan. There are also numerous diffuse areas of high Cl concentration (not as localized as the Cl_{org} hotspots) that are associated with H-bonded Cl_{inorg} (Fig. 3D). Areas of low Cl concentration yield spectra with mixed aliphatic Cl_{org} and Cl_{inorg} speciation (Fig. 3D). Similar Cl μ-speciation characterizes leaves exposed to natural weathering processes for approximately 5 months as part of the mulch layer on the soil surface (Fig. 2).

A highly weathered white oak leaf from the forest floor (estimated weathering time of approximately 2 years) exhibited numerous Cl hotspots (Fig. 3E) encompassing three varieties of Cl μ-speciation: aromatic and aliphatic Cl_{org} and solid phase Cl_{inorg} (Fig. 3F). Of the seven hotspots analyzed, 43% were aromatic Cl_{org} and 43% aliphatic Cl_{org}. Once again, the aliphatic Cl_{org} in the hotspots was easily beam-damaged. The Cl_{inorg} hotspot spectrum (Fig. 3F) is reminiscent of the hotspots commonly observed in unweathered samples (Fig. 3A and B). The diffuse areas of low to moderate Cl concentration in this highly weathered sample consistently produced spectra with H-bonded Cl_{inorg} features (Fig. 3F).

The principal themes of localized aromatic and aliphatic Cl_{org} hotspots and low background concentrations of Cl_{inorg} and aliphatic Cl_{org} throughout the leaf tissue are consistent among all weathering oak leaf samples from various weathering stages. Thus, the most striking change in Cl μ-speciation in fact occurs in the earliest weathering stage, between 0 and 2.5 weeks. Aromatic and, to a lesser extent, aliphatic Cl_{org} hotspots become more prevalent over Cl_{inorg} hotspots in these first weeks of weathering. By contrast, H-bonded Cl_{inorg} appears in diffuse areas of moderate Cl concentration, even in highly weathered leaves (Fig. 3E and F), implying that this pool of Cl_{inorg} either does not leach easily from leaf material or is added as weathering progresses. In weathered leaves, aliphatic Cl_{org} often occurs in areas of low Cl concentration apart from hotspots. This low-concentration aliphatic Cl_{org} does not display X-ray beam damage as the aliphatic Cl_{org} hotspots tend to do, suggesting that the dilute aliphatic Cl_{org} may represent a more stable compound.

NOM samples yield highly variable and complex spectromicroscopic data, in accordance with their intrinsic heterogeneities. As with any synchrotron-based technique, limitations on allotted experimental times preclude acquisition of a statistical dataset. For example, a 10 mm^2 leaf sample can require more than 48 h for detailed mapping of elements and Cl species. Nonetheless, collation of spectromicroscopic data from an assortment of samples reveals salient differences between highly weathered mulch from the forest floor and leaf material in initial weathering stages from our above-ground field station apparatus. In highly weathered NOM from the mulch layers, the majority (54%) of the 63 hotspots analyzed yielded aromatic Cl_{org} spectra, 32% Cl_{inorg}, and 14% aliphatic Cl_{org}. By contrast, only 16% out of the 37 hotspots analyzed in the field station samples were attributable to aromatic Cl_{org}—49% were Cl_{inorg} and 30% aliphatic Cl_{org}. In healthy, unweathered leaves collected from trees, only one (5%) out of the 20 hotspots analyzed gave an aromatic Cl_{org} spectrum—90% of the hotspots in these samples produced Cl_{inorg} spectra. In samples at all stages of weathering, the diffuse areas of low to moderate Cl concentration chiefly gave Cl_{inorg} spectra, sometimes mixed with aliphatic and, less frequently, aromatic Cl_{org} components.

3.3. Solubilities of different Cl_{org} fractions as a function of weathering time

The Cl_{org} in white oak leaves displays variable solubility depending on degree of weathering. A highly weathered white oak leaf (estimated weathering time of approximately one year among soil mulch) displayed several Cl_{org} hotspots of polychlorinated aromatic structure (Fig. 4, map A, spectrum a). After vigorous rinsing with deionized water for

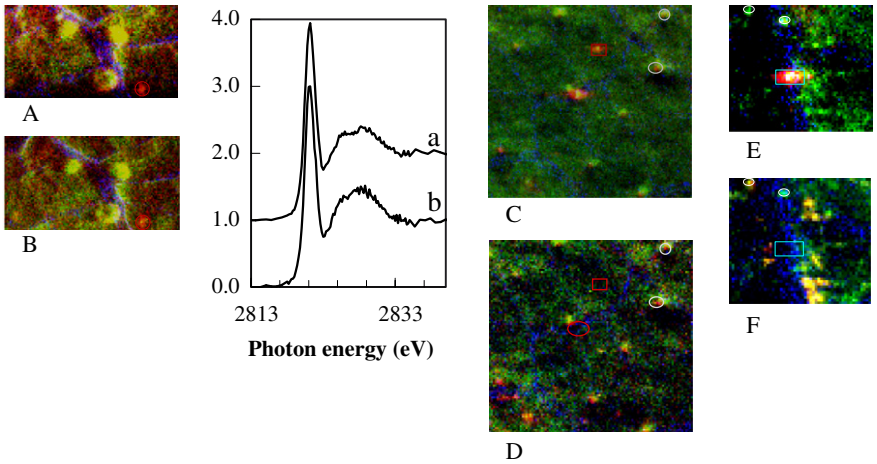

Fig. 4. Variable solubilities of Cl_{org} hotspots in white oak leaves at different weathering stages. In μ-XRF maps (A–F) red = Cl Kα; green = S Kα; blue = Ca Kα. Lighter color corresponds to greater fluorescence intensity, i.e., higher elemental concentration. (A) μ-XRF map of highly weathered white oak leaf surface (estimated weathering time of approximately 1 year among soil mulch). Cl hotspot circled in red corresponds to μ-XANES spectrum "a" (polychlorinated aromatic Cl_{org}). (B) μ-XRF map of same section in (A) after vigorous rinsing with deionized water. The aromatic Cl_{org} hotspot persists in the rinsed sample, yielding μ-XANES spectrum "b", with the same Cl speciation as spectrum "a". The absolute intensities of unnormalized μ-XANES spectra "a" and "b" are identical, indicating no change in concentration of the polychlorinated aromatic hotspot through rinsing. (C) μ-XRF map of lightly weathered white oak leaf surface (weathering time: 2.5 weeks in field station apparatus removed from soil mulch)—*this is a portion of the* μ-*XRF map in Fig. 3C*. The Cl hotspots circled in red correspond to the red spectra in Fig. 3D (polychlorinated aromatic Cl_{org}). (D) μ-XRF map of sample in C after vigorous rinsing with deionized water. The two aromatic Cl_{org} hotspots are not apparent. (E) μ-XRF map of separate segment of sample in (C) (unrinsed)—*another portion of the* μ-*XRF map in Fig. 3C*. The Cl hotspot boxed in turquoise corresponds to the turquoise spectrum in Fig. 3D (aliphatic Cl_{org} speciation). (F) μ-XRF map of sample in E after vigorous rinsing with deionized water. The aliphatic Cl_{org} hotspot is not apparent. (A–F) Maps of the same area differ somewhat in appearance due to acquisition at different resolutions. (C–F) White circles around trichome structures are for spatial orientation.

several minutes, the aromatic Cl_{org} hotspots persist and show unchanged Cl speciation (Fig. 4, map B, spectrum b). The absolute intensities of unnormalized Cl 1*s* μ-XANES spectra of these hotspots before and after rinsing are identical, meaning that rinsing did not diminish the concentration of the polychlorinated aromatic Cl_{org}. The results of this solubility experiment were reproduced for numerous aromatic Cl_{org} hotspots in highly weathered leaf material, indicating that the aromatic Cl_{org} in highly weathered leaves is not easily leachable. By contrast, Cl_{org} in the lightly weathered white oak leaf from the field station experiment (weathering time: 2.5 weeks; see Fig. 3C and D) proved easily leachable. Aromatic and aliphatic Cl_{org} hotspots disappeared upon rinsing (Fig. 4C–F).

These measurements revealed fundamental differences in the solubility of Cl_{org} in highly weathered leaf matter from the soil mulch vs. senescent leaf material in the earliest stages of weathering. Aromatic Cl_{org} occurs in two distinct fractions in decaying NOM. The insoluble aromatic Cl_{org} in highly weathered leaf material may form part of a stable macromolecular structure or be adsorbed to the leaf surface. The soluble aromatic Cl_{org} in the lightly weathered leaf may represent chlorinated counterparts of the relatively low molecular weight polyphenolic molecules that leach from leaves in the first few weeks of weathering.

3.4. Correlations of Cl_{org} with Fe and Mn

Elemental correlations are inconsistent among samples because weathering plant material is highly heterogeneous. For most NOM samples, this heterogeneity makes it impossible to deduce correlations from overall elemental distributions or Pearson-style correlation coefficients. In these cases it proves more fruitful to examine elemental correlations at specific points of interest as identified by Cl 1*s* μ-XANES spectra. The aromatic Cl_{org} hotspots identified in Fig. 2, for example, coincide with spots of elevated Fe concentration (Fig. 5A–C). No other element appears at conspicuously high concentration in the positions of the aromatic Cl_{org} hotspots (Fig. 5D–F). Conspicuous correlations among aliphatic Cl_{org} and other elements were not generally observed.

The correlation of aromatic Cl_{org} hotspots with Fe hotspots was observed in numerous weathered leaf samples. However, one highly weathered sample showed an interesting deviation from this trend. In this white oak leaf from the bottommost mulch layer (estimated weathering time of approximately two years), Cl, Mn, and Fe occur in varied distribution patterns, with an observable association between Cl and Mn but no apparent coincidence of Cl and Fe (Fig. 6A–C). To quantify the associations of our element of interest, Cl, with other elements in the Fig. 6 maps, pixel-by-pixel Pearson *r* correlation coefficients (Manceau et al., 2002) were calculated for different element pairs. The Pearson *r* correlation coefficient quantifies the degree to which two elemental distributions are related, either inversely or directly, with a range of −1.00 to +1.00. Positive correlations were discovered between Cl and the following elements: Mn (0.48), Ca (0.39), Cr (0.28), and Cu (0.21). No apparent correlations exist between Cl and Si, Fe, Ni, or

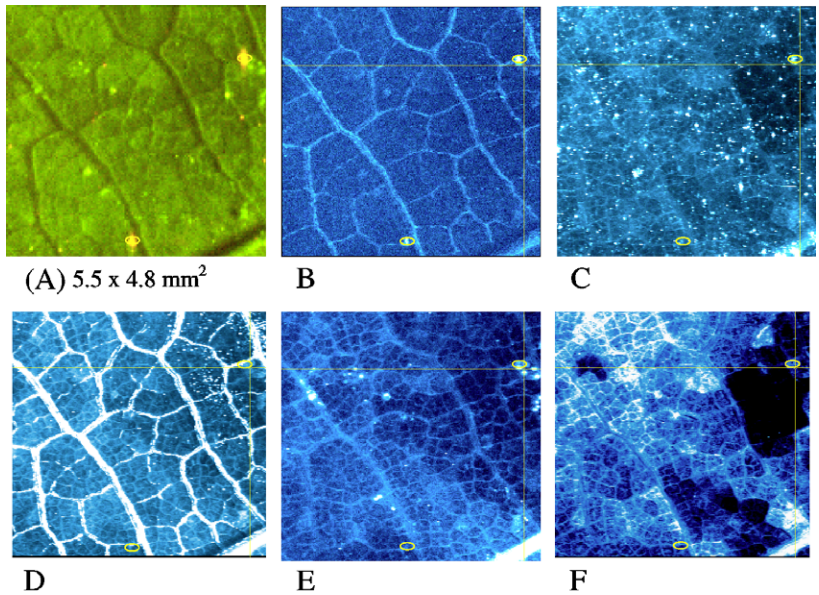

Fig. 5. Elemental distributions in a weathered chestnut oak leaf from the forest floor mulch (estimated weathering time of approximately 5 months). (A) Upper left quadrant of Fig. 2A. (B–F) Monochromatic elemental distributions with yellow ovals in the positions of the aromatic Cl_{org} hotspots identified in Fig. 2. (B) Cl Kα; (C) Fe Kβ; (D) Ca Kα; (E) Zn Kα/Cu Kβ; (F) Mn Kα.

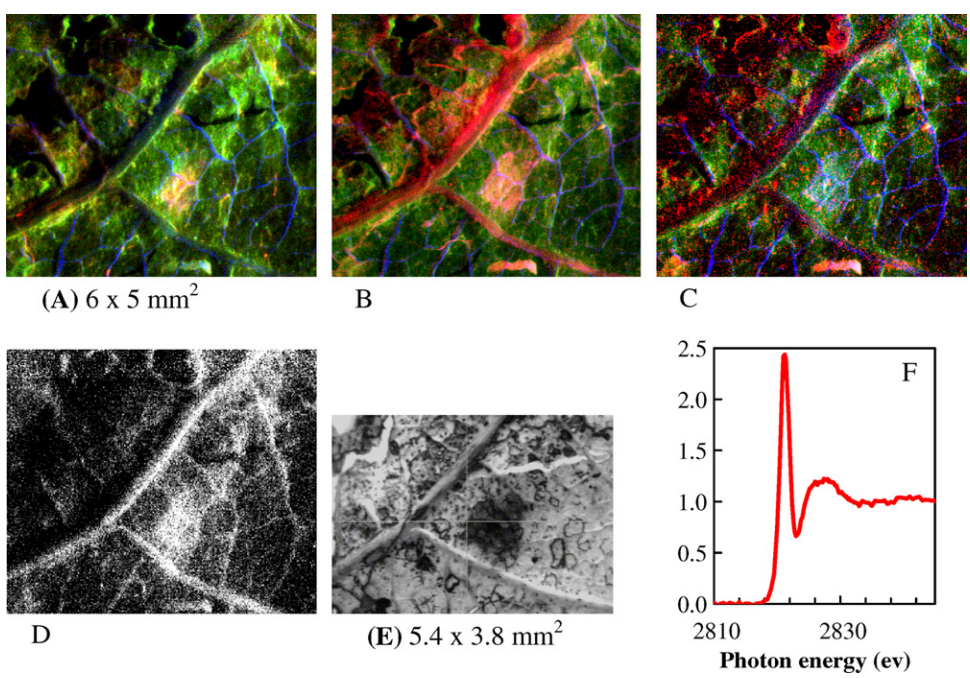

Fig. 6. μ-XRF maps (A–D) of an extremely weathered white oak leaf from the forest floor mulch (estimated weathering time of approximately 2 years). Lighter color corresponds to greater fluorescence intensity, i.e., greater elemental concentration. (A–C) Green = S Kα; blue = Ca Kα; red = variable emission: A) Cl Kα; (B) Mn Kα; (C) Fe Kβ. (D) Elastic scattering distribution. (E) Optical microscopic image of leaf surface. (F) Cl 1s XANES spectrum acquired at central Cl hotspot in map (A) (aromatic Cl_{org} speciation).

Ti. The Cl–Mn correlation has the highest Pearson r coefficient, providing quantitative corroboration of our visual observations.

Optical microscopy revealed that the central area of coincidental Cl and Mn enrichment also overlaps with a fungal mass on the leaf surface (Fig. 6E). The Cl μ-speciation in this central area was revealed to be strongly aromatic Cl_{org} (Fig. 6F). Thus, in this extremely weathered sample, we observed a definitive correlation between aromatic Cl_{org}, Mn, and fungi. This sample was the only one out of the dozen analyzed to display measurable Pearson r correlations between Cl and other elements—

perhaps due to its extraordinary degree of fungal colonization.

3.5. Laboratory-based fungal inoculation of healthy leaves

Inoculation of detached, healthy white oak leaves with the pathogenic fungus *F. oxysporum* in the laboratory (Fig. 7A) resulted in transformation of the Cl_{inorg} endemic to the leaf material (Fig. 7B, a) to aromatic Cl_{org} (Fig. 7B, b), as detected by bulk Cl 1*s* XANES spectroscopy. (The pure *F. oxysporum* culture yielded a strong Cl_{inorg} spectrum, owing to the salt composition of the growth medium.) The post-edge spectral features in *F. oxysporum*—produced aromatic Cl_{org} bear a distinct resemblance to those in the aromatic Cl_{org} hotspots observed in weathered leaves from the forest floor. This result further implicates fungi in the production of aromatic Cl_{org} in decaying plant material, which resonates with recent evidence that fungi chlorinate aromatic rings as they degrade lignin (Ortiz-Bermúdez et al., 2007).

3.6. Scanning electron microscopy of oak leaf surfaces at progressive weathering stages

The spectromicroscopic data presented above may be partially explained by electron microscopic observations of weathered leaf surfaces (Fig. 8). The surfaces of fresh, unweathered oak leaves display a profusion of branched trichomes (Fig. 8A and B). These trichomes are associated with the fairly uniformly distributed spots of high overall fluorescence intensity apparent in the μ-XRF map (Fig. 3A). Such areas tend to exhibit Cl 1*s* μ-XANES features consistent with Cl_{inorg} in either a salt matrix (e.g., Fig. 3B, pink spectrum) or some H-bonded state (e.g., Fig. 3B, green spectrum). Apart from the trichomes, the surface of the unweathered leaf appears even, with some scattered bacteria but no substantial microbial presence (Fig. 8C).

After several months of weathering on the forest floor, oak leaves have had most trichomes sloughed off (Fig. 8D), and their surfaces appear visibly weathered, with evidence of physical damage to the leaf tissue as well as a greater occurrence of microorganisms (Fig. 8E and F). After several years of weathering, trichomes are no longer apparent (Fig. 8G) and substantial fungal colonization of the leaf surface is evident (Fig. 8H and I). Spectromicroscopic analysis of the highly weathered leaf in Fig. 8G–I, showed an abundance of aromatic and aliphatic Cl_{org} hotspots, which may be associated with the fungi apparent on the leaf surface (Fig. 3E and F).

4. SUMMARY AND IMPLICATIONS FOR THE FORMATION OF DIFFERENT Cl_{ORG} POOLS IN NOM

While past bulk X-ray studies demonstrated that aliphatic/aromatic Cl_{org} and Cl_{inorg} appear consistently in weathering plant material (Myneni, 2002a), the results reported here depict Cl speciation variations at the micron scale, revealing the localization of certain Cl species in concentrated hotspots and correlations of these species with other elements and microbiological activity. Detailed spectromicroscopic analyses of numerous leaf samples at different weathering stages enabled us to identify several distinct pools of Cl: (1) concentrated solid phase Cl_{inorg} and H-bonded Cl_{inorg} in tree-harvested oak leaves that diminish in the earliest weathering stages; (2) soluble aromatic and aliphatic Cl_{org} in oak leaves during the earliest weathering stages; (3) insoluble, concentrated aromatic Cl_{org} in oak leaves at advanced weathering stages; and (4) diffuse areas of H-bonded Cl_{inorg} and aliphatic Cl_{org} that persist through advanced weathering stages.

The Cl distribution in weathering oak leaf matter from the soil O-horizon includes localized areas of concentrated aromatic and aliphatic Cl_{org} as well as low background concentrations of Cl_{inorg} and aliphatic Cl_{org} throughout the leaf tissue. While Cl_{inorg} generally appears in a diffuse distribu-

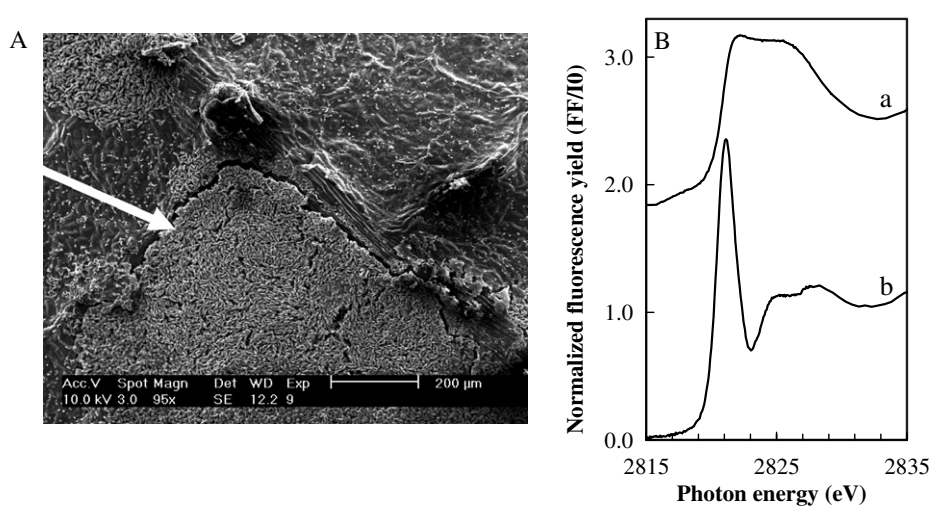

Fig. 7. Effect of induced pathogenic attack on Cl speciation in healthy white oak leaves. (A) SEM image of *F. oxysporum* colony (see arrow) on white oak leaf surface after 2 weeks' incubation. (B) Normalized Cl 1*s* XANES spectra: (a) intact, healthy white oak leaf harvested from tree in the Brendan Byrne State Forest, NJ. (b) white oak leaf after inoculation with *F. oxysporum* and 2 weeks' incubation.

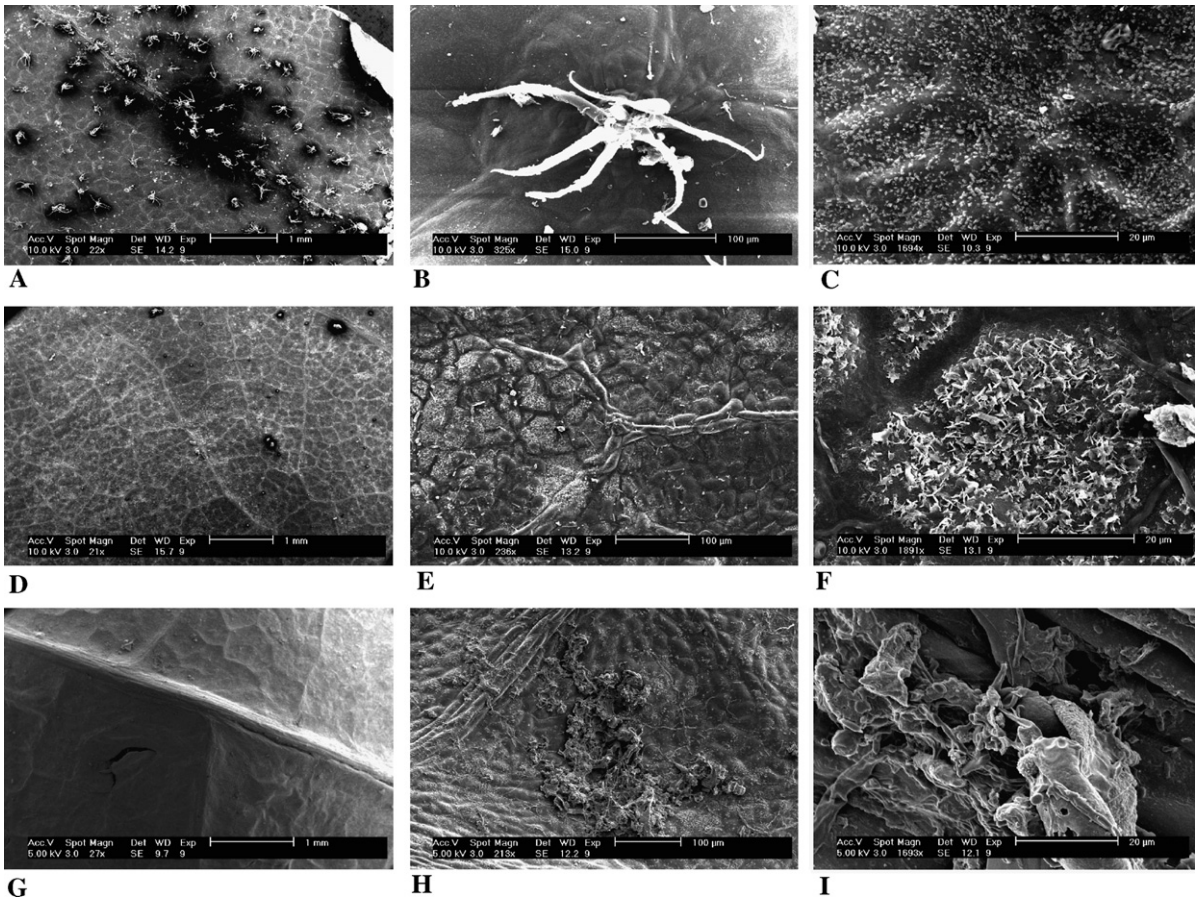

Fig. 8. SEM images of oak leaf surfaces at progressive weathering stages. (A–C) Unweathered white oak leaf harvested from trees. (A) Light-colored raised structures are trichomes. (B) Individual trichome. (C) Leaf tissue between trichomes; apparent wrinkling due to natural topography of leaf surface; scattered bacteria evident. (D–F) Weathered white oak leaf from topmost mulch layer (estimated weathering time of approximately 5 months). (D) Trichomes largely absent from leaf surface. (E and F) Roughened surface tissue; evidence of physical weathering. (G–I) Highly weathered white oak leaf from bottommost mulch layer (estimated weathering time of approximately 2 years). (G) Lack of trichomes. (H and I) Substantial fungal colonization.

tion throughout the leaf tissue, it also occurs in localized hotspots, most often in fresher leaves, the surfaces of which are rich with trichomes that likely play a role in salt excretion in the living plant.

The soluble Cl_{org} hotspots observed in minimally weathered leaves may represent comparatively low molecular weight molecules that leach from leaf material in the earliest weathering stages. In highly weathered leaves from the forest floor, insoluble aromatic Cl_{org} hotspots are common and often coincide with elevated Fe. Metals such as Fe are often the key cofactors in the reaction centers of haloperoxidative enzymes (Sundaramoorthy et al., 1995). In addition, abiotic (non-enzymatic) metal-catalyzed chlorination of aliphatic and aromatic substrates has been documented in natural systems (Keppler et al., 2000; Schoeler and Keppler, 2002; Fahimi et al., 2003; Holmstrand et al., 2006) and as part of biomimetic synthetic schemes in the laboratory (Delaude and Laszlo, 1990; Walker et al., 1997).

Microscopic observations suggest that numerous aromatic Cl_{org} hotspots may be associated with fungal activity on weathered leaf surfaces. In addition, there is a relative lack of insoluble aromatic Cl_{org} hotspots in field station-weathered samples, in which exposure to the soil microbial community is minimized. Finally, laboratory studies in which healthy leaves harvested from trees were subjected to induced weathering by the pathogenic fungus *F. oxysporum* resulted in the conversion of Cl_{inorg} to aromatic Cl_{org}. Together, these results support the assertion that microorganisms play a role in the production of stable aromatic Cl_{org} in NOM. Aromatic moieties are common in NOM and would be susceptible to electrophilic attack and multiple chlorination by a Cl electrophile such as the "Cl^{+}" species known to be released extracellularly by the CPO enzyme (Libby et al., 1992). The breakdown of lignin has been shown to be facilitated by Fe- and V-based fungal CPO, with high molecular weight aromatic Cl_{org} molecules as possible byproducts (Ortiz-Bermúdez et al., 2003). The insoluble aromatic Cl_{org} we observe in highly weathered oak leaves from the forest floor may therefore represent chlorinated macromolecules that result from the oxidative breakdown of plant material by microorganisms.

The highly weathered white oak leaf sample in Fig. 6 is an anomalous but interesting case. It displayed a strong association between aromatic Cl_{org}, Mn, and microscopically observed fungi. Mn-peroxidase enzymes in white-rot fungi often play a key role in lignin degradation (Wariishi et al., 1991; Orth et al., 1993). In addition, numerous strains of white-rot fungi have been associated with the production of aromatic Cl_{org} (de Jong et al., 1992, 1994). It has been posited that the formation of organohalogens is causally related to the degradation of recalcitrant organic matter such as lignin, with exo-enzymatic reactive Cl species, e.g. hypochlorous acid (HOCl), as agents of oxidative breakdown (Öberg et al., 1997). The associations discovered in the Fig. 6 sample bolster this argument.

Aliphatic Cl_{org} in weathered leaves occurs in both concentrated hotspots and diffuse areas of relatively low Cl concentration. Like their aromatic counterparts, aliphatic molecules in NOM may be subject to electrophilic chlorination during the oxidative breakdown of plant material. However, the low background concentration of aliphatic Cl_{org} observed in leaf tissue suggests that this Cl fraction may not originate solely from localized degradation phenomena and may in fact represent an endemic component of weathered leaf tissue.

This spectromicroscopic study provides evidence for several different classes of Cl_{org} in soil NOM as well as different processes leading to their formation. These findings offer new mechanistic insight into Cl transformations in soil NOM, setting the stage for future investigation of the specific microorganisms associated with Cl_{org} production and for bulk chemical analyses of the solubility/mobility vs. insolubility/stability of the various forms of natural Cl_{org}.

ACKNOWLEDGMENTS

Financial support for this work was provided by the U.S. Department of Energy, Office of Basic Energy Sciences (DOE-BES) Chemical and Geosciences Programs, the National Science Foundation (NSF) Chemical Sciences Program, and an NSF Graduate Research Fellowship (A.C.L.). Use of the Advanced Light Source at Lawrence Berkeley National Laboratory was supported by the DOE-BES Materials Sciences Division under Contract No. DE-AC03-76SF00098. A.C.L. thanks Mark Davidson and Jane Woodruff for microscopy training, Michael Hay for help with sample/data collection, and Sirine Fakra for assistance with μ-XRF measurements on ALS beamline 10.3.2. The authors are grateful to Dr. Rodger Harvey and three anonymous reviewers for constructive advice on this manuscript.

REFERENCES

Asplund G., Christiansen J. V. and Grimvall A. (1993) A chloroperoxidase-like catalyst in soil: detection and characterization of some properties. *Soil Biol. Biochem.* **25**, 41–46.

Asplund G. and Grimvall A. (1991) Organohalogens in nature, more widespread than previously assumed. *Environ. Sci. Technol.* **25**, 1346–1350.

Asplund G., Grimvall A. and Pettersson C. (1989) Naturally produced organic halogens (AOX) in humic substances from soil and water. *Sci. Total Environ.*(81/82), 239–248.

Bergbreiter D. E. and Srinivas B. (1992) Peakfit—Version 3.01. *J. Am. Chem. Soc.* **114**(20), 7961–7962.

Boyd, H.P. (1991) A field guide to the Pine Barrens of New Jersey: its flora, fauna, ecology, and historic sites. Plexus Pub.

Christophersen N. and Neal C. (1990) Linking hydrological, geochemical and soil processes on the catchment scale: an interplay between modelling and fieldwork. *Water Resour. Res.* **26**, 3077–3086.

de Jong E., Field J. A., Dings J. A. F. M., Wijnberg J. B. P. A. and de Bont J. A. M. (1992) De novo biosynthesis of chlorinated aromatics by the white-rot fungus Bjerkandera sp. BOS55. *FEBS Lett.* **305**, 220–224.

de Jong E., Field J. A., Spinnler H.-A., Wijnberg J. B. P. A. and de Bont J. A. M. (1994) Significant biogenesis of chlorinated aromatics by fungi in natural environments. *Appl. Environ. Microbiol.* **60**, 264–270.

Delaude L. and Laszlo P. (1990) Aromatic chlorination of toluene and of anisole using clay-supported iron(Iii) chloride and M-chloroperbenzoic acid—a biomimetic approach. *Catal. Lett.* **5**(1), 35–44.

Derby N. E. and Knighton R. E. (2001) Field-scale preferential transport of water and chloride tracer by depression-focused recharge. *J. Environ. Qual.* **30**(1), 194–199.

Engvild K. C. (1986) Chlorine-containing natural compounds in higher plants. *Phytochemistry* **25**(4), 781–791.

Fahimi I. J., Keppler F. and Schoeler H. F. (2003) Formation of chloroacetic acids from soil, humic acid and phenolic moieties. *Chemosphere* **52**(2), 513–520.

Flodin C., Johansson E., Borén H., Grimvall A., Dahlman O. and Mörck R. (1996) Chlorinated structures in high molecular weight organic matter isolated from fresh and decaying plant material and soil. *Environ. Sci. Technol.* **9**, 2464–2468.

Gribble G. W. (2003) The diversity of naturally produced organohalogens. *Chemosphere* **52**(2), 289–297.

Hjelm O., Johansson M. B. and Öberg-Asplund G. (1995) Organically bound halogens in coniferous forest soil—distribution pattern and evidence of in situ production. *Chemosphere* **30**, 2353–2364.

Holmstrand H., Gadomski D., Mandalakis M., Tysklind M., Irvine R., Andersson P. and Gustafsson O. (2006) Origin of PCDDs in ball clay assessed with compound-specific chlorine isotope analysis and radiocarbon dating. *Environ. Sci. Technol.* **40**(12), 3730–3735.

Johansson E., Sandén P. and Öberg G. (2003) Organic chlorine in deciduous and coniferous forest soil, southern Sweden. *Soil Sci.* **168**(5), 347–355.

Keppler F., Eiden R., Niedan V., Pracht J. and Schöler H. F. (2000) Halocarbons produced by natural oxidation processes during degradation of organic matter. *Nature* **403**, 298–301.

Laturnus F., Mehrtens G. and Grøn C. (1995) Haloperoxidase-like activity in spruce forest soil—a source of volatile halogenated organic compounds?. *Chemosphere* **31** 3709–3719.

Leri A. C., Hay M. B., Lanzirotti A., Rao W. and Myneni S. C. B. (2006) Quantitative determination of absolute organohalogen concentrations in environmental samples by X-ray absorption spectroscopy. *Anal. Chem.* **78**(16), 5711–5718.

Libby R. D., Shedd A. L., Phipps A. K., Beachy T. M. and Gerstberger S. M. (1992) Defining the involvement of HOCl or Cl_2 as enzyme-generated intermediates in chloroperoxidase-catalyzed reactions. *J. Biol. Chem.* **267**(3), 1769–1775.

Manceau A., Marcus M. A. and Tamura N. (2002) Quantitative speciation of heavy metals in soils and sediments by synchrotron X-ray techniques. In *Applications of Synchrotron Radiation*

in Low-Temperature Geochemistry and Environmental Science (eds. P. Fenter and N. C. Sturchio). Reviews in Mineralogy and Geochemistry, Mineralogical Society of America, Washington, DC, vol. 49, pp. 341–428.

Marcus M. A., MacDowell A. A., Celestre R., Manceau A., Miller T., Padmore H. A. and Sublett R. E. (2004) Beamline 10.3.2 at ALS: a hard X-ray microprobe for environmental and materials sciences. *J. Synchrotron Radiat.* **11**, 239–247.

Monde K., Satoh H., Nakamura M., Tamura M. and Takasugi M. (1998) Organochlorine compounds from a terrestrial higher plant: structures and origin of chlorinated orcinol derivatives from diseased bulbs of Lilium maximowiczii. *J. Nat. Prod.* **61**(7), 913–921.

Myneni S. C. B. (2002a) Formation of stable chlorinated hydrocarbons in weathering plant material. *Science* **295**, 1039–1041.

Myneni S. C. B. (2002b) Soft X-ray spectroscopy and spectromicroscopy studies of organic molecules in the environment. In *Applications of Synchrotron Radiation in Low-Temperature Geochemistry and Environmental Science* (eds. P. Fenter and N. C. Sturchio). Reviews in Mineralogy and Geochemistry, Mineralogical Society of America, Washington, DC, vol. 49, pp. 485–579.

Niedan V., Pavasars I. and Oberg G. (2000) Chloroperoxidase-mediated chlorination of aromatic groups in fulvic acid. *Chemosphere* **41**(5), 779–785.

Öberg G. (1998) Chloride and organic chlorine in soil. *Acta Hydrochem. Hydrob.* **26**, 137–144.

Öberg G. (2002) The natural chlorine cycle—fitting the scattered pieces. *Appl. Microbiol. Biotechnol.* **58**(5), 565–581.

Öberg G., Brunberg H. and Hjelm O. (1997) Production of organically bound halogens during degradation of birch wood by common white-rot fungi. *Soil Biol. Biochem.* **29**, 191–197.

Öberg G. and Grøn C. (1998) Sources of organic halogens in spruce forest soil. *Environ. Sci. Technol.* **32**, 1573–1579.

Öberg G., Holm M., Sanden P., Svensson T. and Parikka M. (2005) The role of organic-matter-bound chlorine in the chlorine cycle: a case study of the Stubbetorp catchment, Sweden. *Biogeochemistry* **75**(2), 241–269.

Öberg G., Nordlund E. and Berg B. (1996) In situ formation of organically bound halogens during decomposition of Norway spruce litter - effects of fertilization. *Can. J. Forest Res.* **26**, 1040–1048.

Orth A. B., Royse D. J. and Tien M. (1993) Ubiquity of lignin-degrading peroxidases among various wood-degrading fungi. *Appl. Environ. Microbiol.* **59**(12), 4017–4023.

Ortiz-Bermúdez P., Hirth K. C., Srebotnik E. and Hammel K. E. (2007) Chlorination of lignin by ubiquitous fungi has a likely role in global organochlorine production. *Proc. Natl. Acad. Sci. USA* **104**(10), 3895–3900.

Ortiz-Bermúdez P., Srebotnik E. and Hammel K. E. (2003) Chlorination and cleavage of lignin structures by fungal chloroperoxidases. *Appl. Environ. Microbiol.* **69**, 5015–5018.

Reina R. G., Leri A. C. and Myneni S. C. B. (2004) ClK-edge X-ray spectroscopic investigation of enzymatic formation of organochlorines in weathering plant material. *Environ. Sci. Technol.* **38**(3), 783–789.

Ressler T. (1998) WinXAS: a program for X-ray absorption spectroscopy data analysis under MS-Windows. *J. Synchrotron Radiat.* **5**, 118–122.

Schoeler H. F. and Keppler F. (2002) Abiotic formation of organohalogens during early diagenetic processes. *Handbook of Environ. Chem.* **3(P)**, 63–84.

Shadle S. E., Hedman B., Hodgson K. O. and Solomon E. I. (1995) Ligand K-edge X-ray-absorption spectroscopic studies—metal–ligand covalency in a series of transition-metal tetrachlorides. *J. Am. Chem. Soc.* **117**(8), 2259–2272.

Sundaramoorthy M., Terner J. and Poulos T. L. (1995) The crystal structure of chloroperoxidase: a heme peroxidase-cytochrome P450 functional hybrid. *Structure* **3**(12), 1367–1377.

Thomson W. W. and Healey P. L. (1984) Cellular basis of trichome secretion. In *Biology and Chemistry of Plant T richomes* (eds. E. Rodriguez, P. L. Healey and I. Mehta). Plenum Press, NY, p. 255.

Turner W. B. and Aldridge D. C. (1983) *Fungal metabolites*, second ed. Academic Press, NY.

Walker J. V., Morey M., Carlsson H., Davidson A., Stucky G. D. and Butler A. (1997) Peroxidative halogenation catalyzed by transition-metal-ion-grafted mesoporous silicate materials. *J. Am. Chem. Soc.* **119**(29), 6921–6922.

Wariishi H., Valli K. and Gold M. H. (1991) Invitro depolymerization of lignin by manganese peroxidase of phanerochaete-chrysosporium. *Biochem. Biophys. Res. Commun.* **176**(1), 269–275.

White P. J. and Broadley M. R. (2001) Chloride in soils and its uptake and movement within the plant: a review. *Ann. Bot.* **88**(6), 967–988.

Wijnberg J. B. P. A. (1998) Identification and synthesis of novel chlorinated *p*-anisylpropanoid metabolites from Bjerkandera species. *J. Nat. Prod.* **61**, 1110–1114.

Yosioka I., Yamauchi H., Morimoto K. and Kitatgawa I. (1968) Three new chlorine containing bisanthronyls from a lichen, *Anaptychia obscurata* Vain. *Tetrahedron Lett.* **34**, 3749–3752.